Chemical Engineering Journal 522 (2025) 167803

Contents lists available at ScienceDirect

Chemical Engineering Journal

journal homepage: www.elsevier.com/locate/cej

Photoresponsive azobenzene-grafted thermoplastic elastomers with controlled hard segment ratios for fast-rewritable and tunable surface relief gratings

Ming-Chieh Lin, Wen-Kai Cheng, Mohamed Gamal Mohamed, Wei-Hung Su, Shiao-Wei Kuo *

Department of Materials and Optoelectronic Science, Center for Functional Polymers and Supramolecular Materials, National Sun Yat-sen University, Kaohsiung 804, Taiwan

ARTICLE INFO

Keywords:
Thermoplastic elastomer
Hydrogen bonding
Azobenzene
Hard segment
Surface relief grating

ABSTRACT

In this study, thermoplastic elastomers (TPEs) are synthesized based on glycidyl azide polymer (GAP) via step-growth polymerization. Azobenzene moieties are subsequently introduced through a click reaction, enabling the preparation of a series of thermoplastic elastomers (GAP-TPE) with varying azobenzene contents and hard segment ratios, offering tailored optical response and thermomechanical properties. By grafting azobenzene moieties at different loadings, the diffraction efficiency of the materials shows a significant enhancement, resulting in the successful fabrication of a series of azobenzene-grafted thermoplastic elastomers (GAP-TPE-AZO) capable of forming surface relief gratings (SRGs) through photoinduced trans-cis isomerization. By tuning the hard segment ratio of the thermoplastic elastomers, a wide range of controllable grating amplitudes can be achieved, with GAP-TPE_{50}-AZO_{30} exhibiting the highest surface relief grating (SRG) depth of up to 687 nm. On the other hand, GAP-TPE_{50}-AZO_{30} also demonstrates rapid grating erasure within 1 min upon heating above its softening point, and the grating can be rewritten repeatedly. Therefore, owing to the combination of tunable grating amplitude, excellent rapid erasure, and rewritability, these findings highlight the significant potential of such materials in advancing next-generation rewritable optical storage technologies.

1. Introduction

Photoresponsive polymers are increasingly utilized in a variety of modern technologies, including photoactuators, drug delivery systems, and anti-counterfeiting labels. [1–5] Additionally, in the fields of information storage and optical components, they can be applied to rewritable optical discs, holographic data storage devices, and liquid crystal modulators. [6–8] Among them, the use of light-induced deformation to fabricate micro/nanoscale surface relief gratings (SRGs) holds great application potential in holographic data storage and rewritable memory. Furthermore, the grating amplitude and the ability for rapid erasure directly affect the feasibility and advantages of SRG materials in these application fields. [9,10] In rewritable optical storage devices, as well as the requirement for grating amplitude, greater emphasis is placed on the writing and erasure efficiencies. Among photoresponsive molecules, azobenzene is the most widely used due to its reversible trans-cis isomerization behavior and excellent reversibility. [11–14] Nevertheless, its high crystallinity makes it difficult to process on its own. Therefore, azopolymers, due to their high reactivity and excellent film-forming properties, have further expanded the opportunities for their applications.

The formation of SRGs primarily relies on the isomerization and molecular reorientation of azobenzene-containing materials. Upon irradiation with light of a specific energy, the induced molecular rearrangement leads to refractive index modulation, followed by mass migration at constructive interference regions and mass accumulation at destructive interference regions, eventually forming the grating structure. [11,15] When azobenzene derivatives form covalent or non-covalent bonds with polymers, the structural and volumetric differences between the trans and cis isomers can induce overall molecular motions at the nanoscale, which ultimately display as macroscopic deformations and the formation of SRGs. [16,17] From numerous studies on azopolymers, it is apparent that the glass transition temperature (T_g) is a critical parameter for SRG stability. SRGs formed in these non-crystalline azopolymers can be erased by thermal treatment, and the required erasure temperature closely corresponds to the material's T_g.

* Corresponding author.
E-mail address: kuosw@faculty.nsysu.edu.tw (S.-W. Kuo).

https://doi.org/10.1016/j.cej.2025.167803
Received 4 July 2025; Received in revised form 18 August 2025; Accepted 26 August 2025
Available online 28 August 2025

[10,18,19] Research on the control of SRG amplitude and rapid erasure capability is ongoing. [9,10,20] Although SRGs formed via azopolymers have attracted interest, systematic studies on their performance remain limited. There is considerable potential in developing simplistic and efficient materials with controllable SRG amplitudes.

Thermoplastic elastomers (TPEs) are polymeric materials that combine the elastic properties of rubber with the processability of thermoplastics. They offer advantages such as reprocessability, recyclability, and feasibility of property tuning. Thus, TPEs are widely used in the automobile industry, electronic devices, consumer goods, and biomedical materials. [21–29] Specific polyols are commonly used as soft segment materials, while isocyanates and small molecule chain extenders (usually diols or diamines) are used as hard segment compositions. By adjusting the ratio of these components, thermoplastic elastomers with varying soft and hard segment contents can be synthesized, allowing precise tuning of their thermal properties, crystallinity, and mechanical performance. [30–34] Regarding crystalline behavior, thermoplastic elastomers sometimes exhibit two distinct glass transition temperatures. One at a lower temperature transition corresponds to the crystallization of the soft segment, and the other at a higher temperature transition results from the hydrogen-bonded polyurethane between hard segments. While the temperature rises, triggering these hydrogen bonds to dissociate, the crystalline structure of the hard segments is disrupted, permitting molecular mobility. Therefore, this higher transition temperature can also be regarded as the softening point of the elastomer. [35–37] A commonly used way to erase the SRGs formed by these materials is thermal treatment, such as heating above their glass transition temperature. However, the erasure process is typically slow (ranging from tens of minutes to several hours), and the materials are often costly and difficult to process during fabrication. [10,38] Therefore, rapid transition from solid to flowable state upon reaching the softening point of thermoplastic elastomers expresses a valuable property in this field. In addition, their low material cost and facile tunability of soft and hard segment ratios during synthesis make them a promising candidate as a matrix for SRGs applications.

In previous studies, azobenzene derivatives have been incorporated into both the main chain and side chains of polymers to synthesize azopolymers capable of generating SRGs. [39,40] However, the resulting gratings typically exhibited limited amplitude and poor erasure efficiency upon thermal treatment. Based on previous studies, our objective is to synthesize a thermoplastic elastomer incorporating azido functional groups onto the polymer structure. The synthesis of thermoplastic elastomers containing various ratios of azobenzene moieties was achieved by click chemistry in a rapid, straightforward, high-yield, and controllable way. [41] Thus, through a sequence of cationic ring-opening polymerization, step-growth polymerization, and click chemistry, azobenzene moieties were successfully grafted onto the side chains of thermoplastic elastomers, resulting in elastomers with different hard segment ratios and azobenzene contents. By comparison with the diffraction efficiency and SRG amplitude of these elastomers, the interpretations of these results have been given. The hydrogen bonding interactions generated by the polyurethane segments give these elastomers a softening point, which facilitates thermal flowability and rapid erasure of the gratings, enabling erasure rapidly. These findings demonstrate that thermoplastic elastomers are suitable materials for generating SRGs with tunable amplitude and rapid erasability, making them promising candidates for next-generation rewritable data storage applications.

2. Experimental

2.1. Materials

2-(Chloromethyl) oxirane (Epichlorohydrin, 99 %), boron trifluoride etherate (BTFE, 98 %), dibromoneopentyl glycol (98 %), 4,4′-Methylenebis (cyclohexyl isocyanate) (H_{12}MDI, 90 %, mixture of isomers), 1,4-butanediol (1,4-BDO), Propargyl bromide, 4-phenylazophenol (98 %), and sodium L-ascorbate (99 %) were obtained from Thermo Scientific. Dichloromethane (DCM, 99.5 %), *N, N*-dimethylformamide (DMF, 99.8 %), n-hexane (99.5 %), tetrahydrofuran (THF), and ethyl acetate (EA) were procured from Acros Organics and are of analytical grade. Sodium chloride (99.5 %), magnesium sulfate (anhydrous, 99 %), sodium azide (NaN_3), potassium carbonate (K_2CO_3), and copper sulfate ($CuSO_4$, 99 %) were purchased from SHOWA. Dibutyltin dilaurate (DBTDL, >95.0 %) was sourced from Tokyo Chemical Industry. Triethylamine (TEA, 99 %), tert-butanol, acetone (99 %), and methanol (99.8 %) were obtained from DUKSAM. All of the above materials were used without further purification.

2.2. Preparation of polyepichlorohydrin (PECH)

The initiator of dibromoneopentyl glycol (6 g, 22.9 mmol) and 150 mL of dichloromethane (DCM) as a solvent and then, 1 mL of the catalyst of boron trifluoride etherate (BTFE) was dropped, allowing the reaction to proceed at room temperature for about 30 min. (initiator: catalyst = 6 g: 1 mL). Afterward, place the reaction flask in an ice bath at 0 °C and slowly titrate the epichlorohydrin monomer (20 g, 216.2 mmol) into the mixture, which has already been stirred for 30 min at room temperature. The titration process continued for over 4 to 6 h, followed by a 24-h polymerization period. The resulting product, PECH, is dissolved in 150 mL of DCM and extracted three times with 150 mL deionized water containing sodium chloride to eliminate any unconverted compounds, such as the initiator and catalyst. Finally, the organic layer was dehydrated using magnesium sulfate, subjected to filtration, and concentrated by rotary evaporation at 50 °C for about 30 min. The product is then left to dry in vacuo at ambient temperature for 6 h to obtain pure PECH.

2.3. Preparation of glycidyl azide polymer (GAP)

Dissolve 10 g of PECH with 50 mL of dimethylformamide (DMF) and gradually heat the reaction mixture until the polymer is fully dissolved. Gradually add 13 g of sodium azide, maintaining the temperature at 120 °C for 12 h. Afterward, cool the reaction mixture to room temperature to terminate the reaction. Filter the product to remove any unreacted sodium azide and sodium chloride byproducts. Once the DMF solvent is removed by reduced pressure distillation, dissolve the product in dichloromethane. Use an extraction method to wash the solution several times with deionized water. Finally, evaporate the solvent by rotary evaporation at 50 °C, and dry the product in a vacuum oven at room temperature for 6 h to obtain GAP, whose molecular weight was 1270 Da measured by gel permeation chromatography analysis.

2.4. Synthesis of (E)-1-phenyl-2-(4-(prop-2-yn-1-yloxy) phenyl) diazene (AZO- Alkyne)

Initially, 4-phenylazophenol (10 g, 50.4 mmol) was added to the flask and dissolved in DMF (200 mL), and K_2CO_3 (2.23 g, 16.1 mmol) was added. Heat the mixture in an oil bath to 100 °C and stir for 30 min. Then, slowly added propargyl bromide (4.8 g, 40.3 mmol) and allowed the reaction to proceed under an inert atmosphere of nitrogen for 24 h. Once the reaction was complete, filter off the K_2CO_3. Removed the solvent using rotary evaporation and purified the residue via column chromatography (silica gel, *n*-hexane: dichloromethane = 1:1). An orange liquid was obtained. The solvent was evaporated under reduced pressure again, and the resulting orange powder was dried under vacuum at room temperature for 24 h, yielding 7.63 g of the product with a yield of 64 %.

2.5. Synthesis of GAP-TPE

GAP polyol acted as a soft segment, which was placed in vacuo at

90 °C to remove moisture for 2 h. 1,4-BDO, the chain extender, as part of the hard segment in polyurethane, was treated in an 80 °C oven for at least 1 h. First, the pretreated GAP was added to a three-neck flask fitted with a mechanical agitator. The setup was conditioned through three vacuum-nitrogen purge cycles to exclude air and moisture. Afterward, DBTDL (0.25 mL), serving as the catalyst, was injected into the reaction flask and mixed well. Subsequently, the reaction mixture was heated to 90 °C. Being part of the hard segment structure, H_{12}MDI was injected into the flask by syringe to minimize contact with humidity in the environment. The reaction then continued for 2 h. Upon the end of the prepolymer reaction, the reaction temperature was cooled down to 60 °C, then 1,4-BDO was injected, and the reaction was kept stirring until a homogeneous mixture was obtained within 5 min. Subsequently, the whole reaction batch was cured at 100 °C in an oven for 24 h. The molar ratio and mass of GAP, H_{12}MDI, and 1,4-BDO utilized in this study and calculations are summarized in Table S1. The hard segment (HS) ratio of GAP-TPE was defined by mass fraction using the following formula $HS\% = (W_{H12MDI}+W_{1,4-BDO})/(W_{H12MDI}+W_{1,4-BDO}+W_{polyol})$ [36,42,43].

2.6. Synthesis of GAP-TPE-AZO

For the typical synthesis steps of GAP-TPE-AZO. Employing a three-neck round-bottom flask fitted with a magnetic stirring bar, thermometer, and reflux condenser, dissolved AZO-Alkyne (2 g, 8.5 mmol) and GAP-TPE (10 g) in a tert-butanol and deionized water solution (1:1 ratio). The reacted mass of GAP-TPE and AZO-Alkyne used in this study and calculation are provided in Table S2. Then, added sodium ascorbate (0.6 g, 3.0 mmol) and $CuSO_4{\cdot}5H_2O$ (0.3 g, 1.2 mmol), stirring for 30 min. After adding TEA (6.25 mL), the mixture was kept reacting for 10 to 12 h at 90 °C. While the reaction was complete, the solvent was poured out, leaving a gel-like residue at the bottom of the flask. Deionized water (10 mL) and concentrated ammonia (2 mL) were then added and stirred for 30 min. Filter the mixture and wash the residue with water. The desired GAP-TPE-AZO appeared as a yellowish-brown gel, which was then placed in a freeze dryer to remove any excess water.

2.7. Preparation of elastomer film

GAP-TPE-AZO was dissolved in THF and deposited onto a 1 cm × 1 cm glass substrate via drop-coating. The film was left undisturbed in a 60 °C oven for approximately 10 min to allow complete evaporation of the solvent. The resulting film had a coating weight of approximately 2.4 mg. The film thickness was measured via a Veeco Dektak 150 surface profiler and found to be 4.00 ± 0.10 μm, as shown in Table S3.

2.8. Surface relief grating fabrication

SRGs fabrication referred to the polarization holographic recording process from a previous publication [44]. To prevent vibration interference and ensure experimental stability, an optical vibration isolation table was employed. A laser beam with a power of 30 mW and a Gaussian distribution profile was split into two beams of equal intensity using a beam splitter. Each beam had a power density of approximately 100 mW/cm^2. The distance from the mirror to the sample was 72 cm, and the laser spot size was 4.4 mm. A diode-pumped solid-state (DPSS) laser provided green light at a wavelength of 532 nm as the interference source, with an incident angle set at 3.5°, while a He—Ne laser emitting red light at 633 nm was used for assessing the diffraction efficiency of the generated SRG.

3. Results and discussion

3.1. Preparation and characterization of GAP-TPE, AZO-Aklyne, and GAP-TEP-AZO polymers

To investigate whether thermoplastic elastomers can effectively form surface relief gratings with the assistance of light-responsive molecules, we designed the main polymer GAP-TPE with azide functional groups distributed in the soft segment, and isocyanate and diol consist of the hard segment. Different AZO content of GAP-TPE-AZO samples were synthesized by grafting a guest molecule AZO, which contains a photoswitchable azobenzene molecule, onto the side chain via the click reaction. The synthesis procedure is summarized in Scheme 1.

Based on our previous research [45], PECH was synthesized as a precursor via cationic ring-opening polymerization and subsequently modified to the glycidyl azide polymer, GAP, as shown in Fig. 1(a). The FTIR spectra confirmed the distinctive peaks of PECH within the fingerprint zone, especially C—Cl and C—Br vibrations at 748 cm^{-1} and 707 cm^{-1}, which can be observed in Fig. 1(b).

Upon completion of the azidation reaction, these halogens were replaced by azido groups, which gave rise to the absence of these absorption peaks. Meanwhile, a prominent absorption band near 2102 cm^{-1} emerged, representing the appearance of azido functionalities, whereas the C—N single bond is also detected near 1280 cm^{-1}. By analyzing the ^{1}H NMR spectra (Fig. 1(c)), proton signals corresponding to the initiator and the epichlorohydrin repeating unit appeared from 3.26 to 3.83 ppm. The resonance at 3.48 ppm is attributed to the -CH_2-Br proton of the initiator, while the resonance at 3.60 ppm stands for the -CH_2-Cl proton belonging to the repeating unit. Upon completion of the azidation, the halogens were substituted with azido groups, resulting in the shift of the proton signal to 3.33 ppm (-CH_2-N_3). The ^{13}C NMR spectra (Fig. 1(d)) clearly distinguish the signals of the ether group. The chemical shifts of the carbon atoms in the -CH_2-Br and -CH_2-Cl groups are observed at 34.48 ppm and 44.10 ppm, respectively. Subsequent to azidation of -CH_2-Br and -CH_2-Cl, the chemical shifts move to 53.15 ppm and 51.50 ppm, respectively. Additionally, those resonances at 66.70–63.10 ppm and 15.24–14.87 ppm may plausibly originate from end-group structures formed via side reactions. In addition to the activated monomer mechanism (AMM), the activated chain end (ACE) mechanism can also occur during polymerization, leading to chain transfer reactions and the formation of ethoxy (-OCH_2CH_3) end groups. [46] This assignment is consistent with the signals observed in Fig. 1(d). Therefore, the FTIR, ^{1}H NMR, and ^{13}C NMR analyses indicated the modification of PECH to yield GAP.

GAP was used as the polyol and reacted with the diisocyanate (H_{12}MDI) and the chain extender of 1,4-BDO to synthesize a thermoplastic elastomer rich in azido functional groups, referred to as GAP-TPE, as shown in Fig. 2(a). In the FTIR spectra shown in Fig. 2(b), a distinct absorption peak near 2101 cm^{-1} assigned to the azide (N_3) functionality was observed, indicating that the azido groups were retained after the synthesis of GAP-TPE. These preserved azido groups are available for succeeding click chemistry reactions. Upon reaction with H_{12}MDI and 1,4-BDO, polyurethane segments were formed, with N—H stretching vibrations appearing around 3350 cm^{-1}. Additional signals at 1708 cm^{-1} and 1668 cm^{-1} can be assigned to the free and disordered carbonyl (C=O) groups in the polyurethane structure. Alkane C—H stretching vibrations were also observed at 2924 cm^{-1} and 2852 cm^{-1}. Then, GAP-TPE underwent a click reaction with AZO-Alkyne through a Huisgen cycloaddition between the azido groups on GAP-TPE and the alkyne groups of AZO-Alkyne, resulting in the grafting of photoresponsive azobenzene molecules onto the side chains of GAP-TPE. The strong signal in the FTIR spectrum at 2128 cm^{-1} assigned to the C≡C stretching vibration of AZO-Alkyne disappeared after the reaction, indicating successful cycloaddition. Moreover, the characteristic C—C stretching peaks within the aromatic ring were observed at 1600 cm^{-1}, 1582 cm^{-1}, and 1498 cm^{-1} in the spectrum of GAP-TPE-AZO after

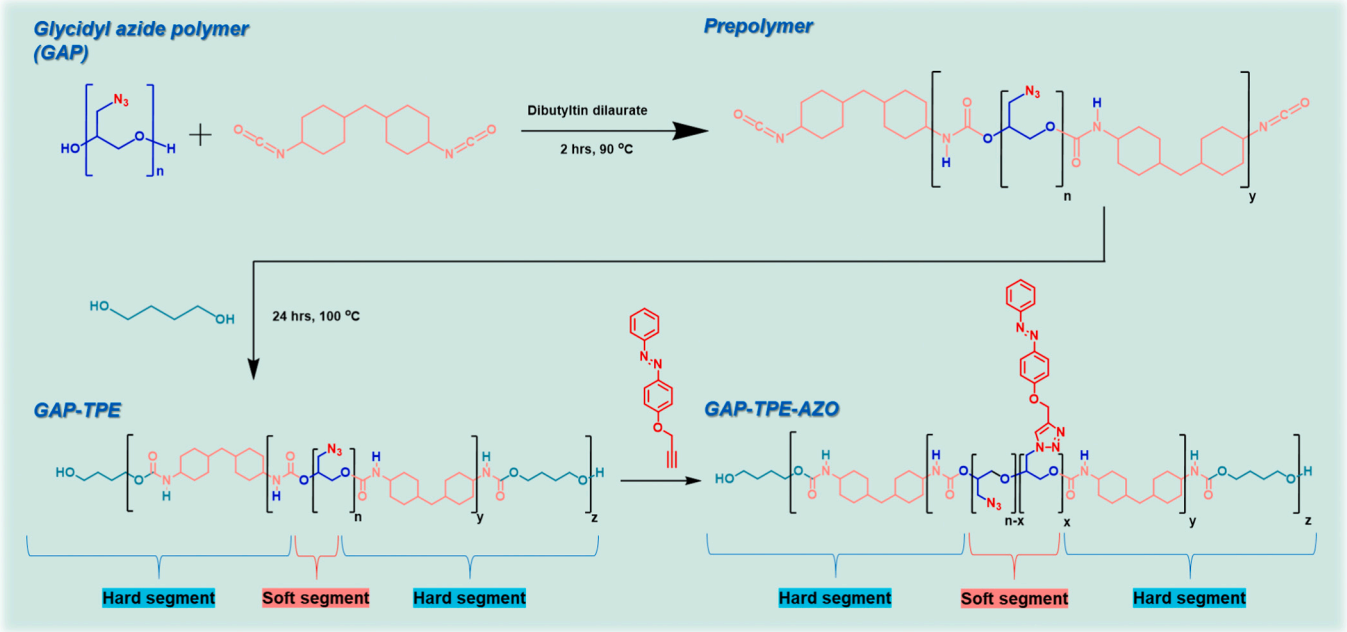

Scheme 1. Synthesis route of GAP-TPE-AZO polymers with various AZO contents

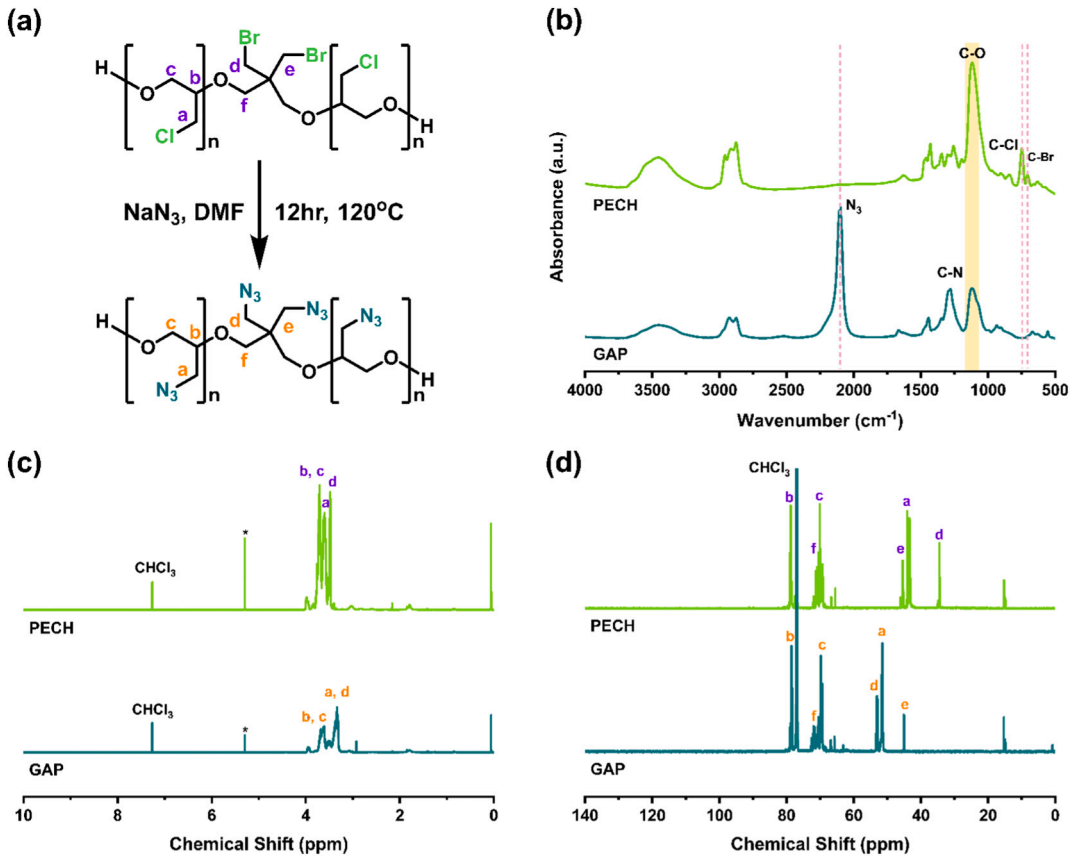

Fig. 1. PECH and GAP of (a) synthesis route; (b) FTIR spectra; (c) ^{1}H NMR, and (d) ^{13}C NMR spectra (*dichloromethane).

the click reaction.

Fig. 2(c) and 2(d) exhibit the NMR characterization results for the synthesized GAP-TPE-AZO. Starting with the synthesis of GAP-TPE, the ^{1}H NMR spectra indicate that the CH_2 signal connecting the cyclohexyl units in H_{12}MDI resonates at 0.96 ppm. Aliphatic resonances from the cyclohexyl rings appear at 3.41, 1.98, and 1.09 ppm, while the proton resonance from the amide N—H group is observed at 4.87 ppm. With 1,4-BDO as the chain extender, the two methylene (C-CH_2-) resonances are seen at 1.67 and 1.55 ppm, besides the -O-CH_2- resonance appears at 3.63 ppm. The -OH end-group proton is detected at 4.06 ppm. Based on

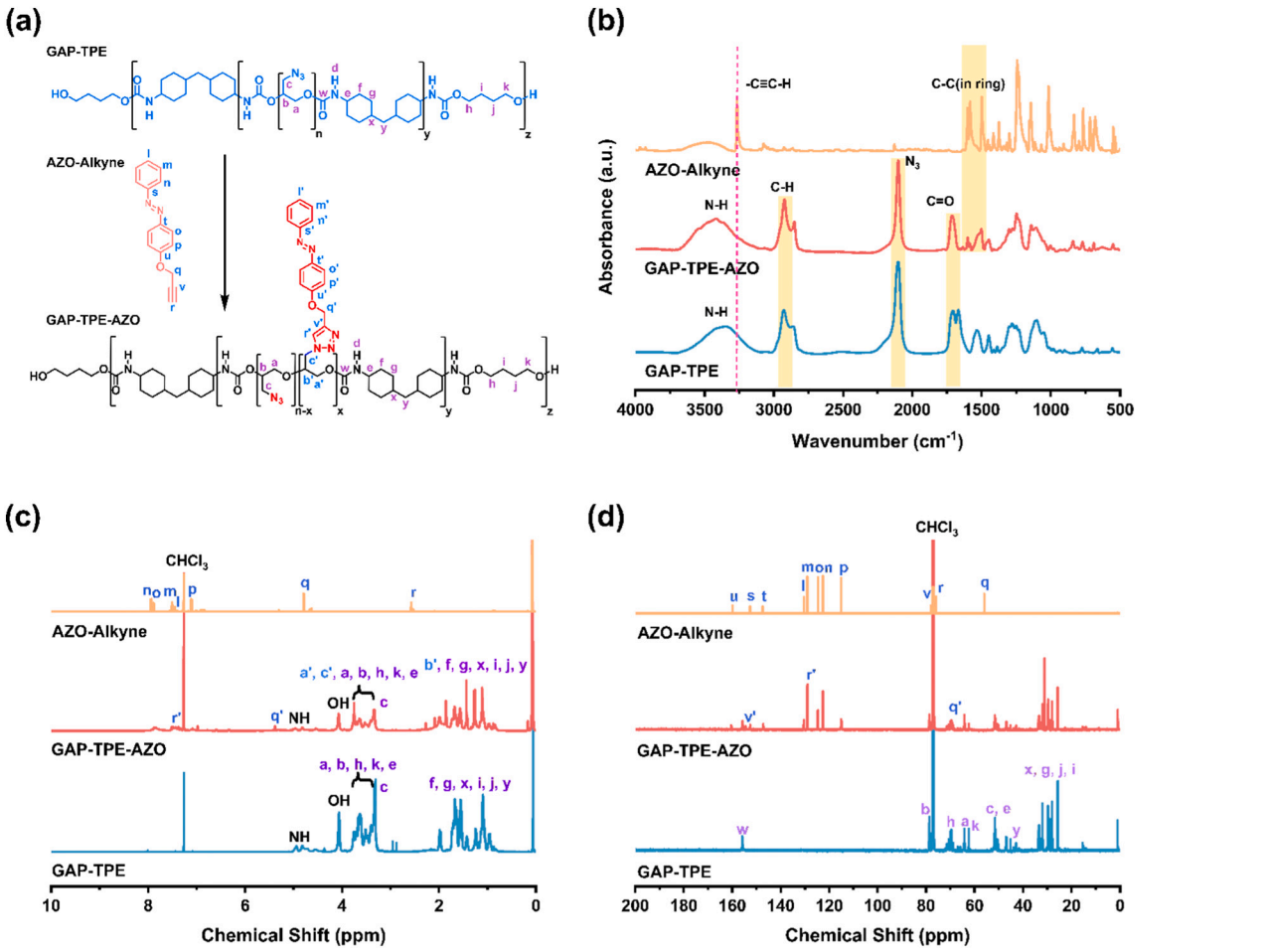

Fig. 2. (a) Synthesis route of GAP-TPE-AZO copolymer from GAP-TPE and AZO-Alkyne by click reaction and their corresponding (b) FTIR, (c) ^{1}H NMR, and (d) ^{13}C NMR spectra.

the ^{13}C NMR spectra, the amide carbon signal appears at 155.79 ppm, and the carbon linking the two cyclohexyl rings is observed at 43.20 ppm. The carbon signals from the cyclohexyl rings of H_{12}MDI are located at 51.55, 33.38, 32.00, and 29.03 ppm. Additionally, signals corresponding to 1,4-BDO appeared at 69.54, 62.38, 27.09 ppm, and 25.67 ppm. After conducting the click reaction with GAP-TPE, the original NMR signals of GAP-TPE remain present, while some of the signals shifted due to the cycloaddition between the azido groups and the terminal alkyne of AZO-Alkyne. Specifically, in the ^{1}H NMR spectra, the terminal alkyne signals of AZO-Alkyne originally at 4.79 and 2.57 ppm shifted downfield to 5.39 and 7.37 ppm after triazole formation. Additionally, the -CH_2- signal adjacent to the newly formed triazole ring appears at 3.75 ppm. In the ^{13}C NMR spectra, the terminal alkyne carbon signals of AZO-Alkyne originally at 78.02, 75.98, and 55.99 ppm significantly shifted to 154.46, 128.57, and 69.13 ppm after the click reaction. These observations, in conjunction with the previously mentioned FTIR analyses, confirm the successful synthesis of GAP-TPE-AZO.

In the synthesis of GAP-TPE, thermoplastic elastomers with different hard segment contents of 40 %, 45 %, and 50 % were prepared. For each composition, AZO-Alkyne was incorporated at 10 wt%, 20 wt%, and 30 wt%, respectively, to undergo the click reaction. The detailed compositions of the reaction formulations are summarized in Tables S1 and S2. The results of GPC analysis are displayed in Fig. S2, with the respective molecular weight results collected in Table 1.

From the GPC results, it was observed that the molecular weight of GAP-TPE increased with a higher hard segment ratio. Additionally, increasing the amount of AZO-Alkyne also led to a further rise in molecular weight. This suggests that increasing the proportion of AZO-Alkyne effectively enhances the degree of azobenzene grafting onto the side chains of the GAP-TPE molecules. Fig. 3(a)-(c) exhibit the ^{1}H NMR spectra for samples with different hard segments and AZO contents. The integrated area of the aromatic -C-H signals belonged to the azobenzene moiety, observed in the range from 7.98 ppm to 7.31 ppm, and increases

Table 1
Characteristics and thermal properties of various GAP-TPE-AZO elastomers.

Sample	M_n (Da)	PDI	AZO ratio* (%)	T_g# (°C)	T_m (°C)
$GAP\text{-}TPE_{40}$	3180	1.77	–	−24.7	61.9
$GAP\text{-}TPE_{40}\text{-}AZO_{10}$	5470	1.52	6.3	−3.3	–
$GAP\text{-}TPE_{40}\text{-}AZO_{20}$	5930	1.49	12.6	7.0	–
$GAP\text{-}TPE_{40}\text{-}AZO_{30}$	6400	1.57	27.8	17.5	–
$GAP\text{-}TPE_{45}$	3990	1.76	–	−23.5	78.4
$GAP\text{-}TPE_{45}\text{-}AZO_{10}$	5880	1.56	6.8	−2.0	85.6
$GAP\text{-}TPE_{45}\text{-}AZO_{20}$	5980	1.43	13.7	8.9	96.2
$GAP\text{-}TPE_{45}\text{-}AZO_{30}$	6220	1.45	30.4	19.2	125.7
$GAP\text{-}TPE_{50}$	4770	1.84	–	−13.1	82.9
$GAP\text{-}TPE_{50}\text{-}AZO_{10}$	6270	1.37	7.5	1.0	96.4
$GAP\text{-}TPE_{50}\text{-}AZO_{20}$	8330	1.28	15.1	9.5	98.9
$GAP\text{-}TPE_{50}\text{-}AZO_{30}$	8680	1.30	33.4	19.8	125.5

* The AZO ratio represents the theoretical conversion of azido groups successfully grafted as azobenzene derivatives through click chemistry, which was calculated using ^{1}H NMR spectra via the model reaction of AZO-Alkyne click reaction on GAP, as shown in Fig. S3.

The glass transition temperature was determined from the derivative of the second-round scanning.

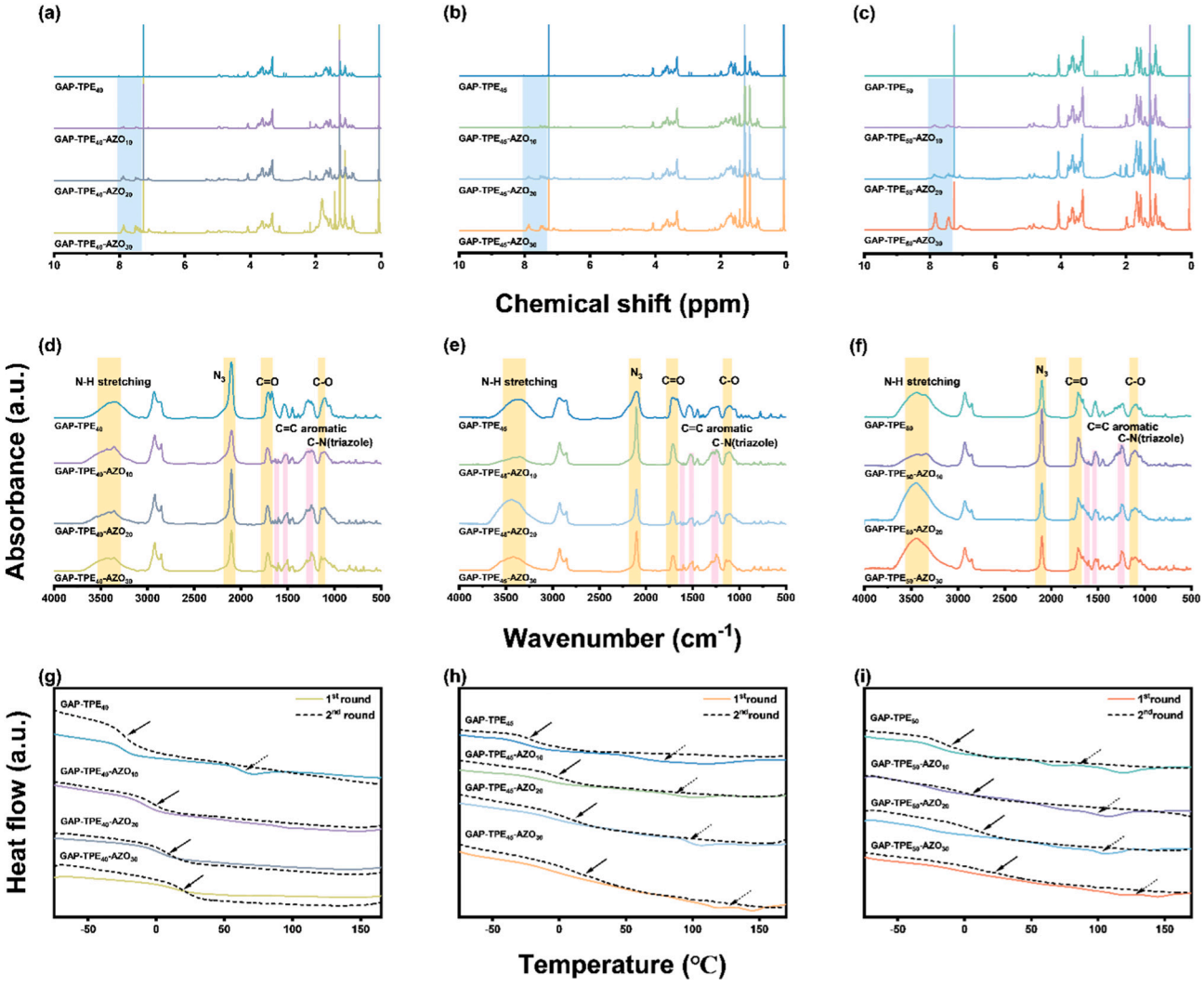

Fig. 3. ^{1}H NMR spectra of various AZO contents for (a) 40 %, (b) 45 %, and (c) 50 % HS GAP-TPE.; FTIR spectra of (d) different AZO content for 40 % HS GAP-TPE, (e) different AZO content for 45 % HS GAP-TPE, and (f) different AZO content for 50 % HS GAP-TPE.; thermal properties of (g) different AZO content for 40 % HS GAP-TPE, (h) different AZO content for 45 % HS GAP-TPE, and (i) different AZO content for 50 % HS GAP-TPE.

with higher AZO-Alkyne loadings. However, due to the overlap and broadness of signals from the GAP-TPE backbone, direct quantification of AZO content in the GAP-TPE-AZO samples via ^{1}H NMR was not feasible. Since the specific high yield of the click reaction, the AZO content of GAP-TPE-AZO was instead estimated based on the equivalent weight percentages of AZO-Alkyne reacted with GAP in model reactions, as presented in Table S2. The estimated AZO content in the final GAP-TPE-AZO samples calculated by the model reaction's results is also summarized in Table 1, indicating the increasing trend of AZO content for each series of GAP-TPE-AZO samples.

The FTIR spectra of GAP-TPE$_{40}$, GAP-TPE$_{45}$, and GAP-TPE$_{50}$ elastomers grafted with different amounts of azobenzene molecules are presented in Fig. 3(d)-(f). Since only part of the azido groups took part in the click reaction, a distinctive absorption band near 2101 cm^{-1}, attributed to the azide functional group, was still observed before and after the reaction. Following the partial grafting of azobenzene derivatives via the click reaction, the intensity of several characteristic peaks increased with the AZO content. Especially, peaks at 1601 cm^{-1} and 1502 cm^{-1} were attributed to C═C (aromatic) stretching vibration, and the peak at 1475 cm^{-1} was related to the triazole ring. [47] Furthermore, the peak at 1247 cm^{-1}, associated with C—N and C═N stretching within the triazole ring, also exhibited enhanced intensity with higher AZO content. [48] Interestingly, the characteristic peaks observed at 1708 cm^{-1} and 1668 cm^{-1} are associated with the free C═O and disordered C═O groups within the amide structure, respectively. Before the click reaction, these two peaks were clearly distinguishable, demonstrating the coexistence of both carbonyl environments. However, after the click reaction, an obvious shift from disordered C═O stretching to free C═O stretching was observed. This shift is presumed to result from the grafting of bulky azobenzene derivative moieties onto the polymer side chains, which increases regional steric hindrance. Thus, hydrogen bonding becomes interrupted or tends not to form, leading to a more prominent free C═O characteristic peak. Under ambient conditions, certain functional moieties present in the thermoplastic elastomers, which were achieved by amide groups in this study, can form hydrogen bonds, resulting in a compact molecular structure that leads to material solidification. [34,49,50] Upon heating, hydrogen bonding is gradually disrupted and eventually dissociates, allowing the polymer to regain flowability. This reversible behavior enables the material to repeat cycles of solidification and flow governed by temperature, thus imparting thermoplastic properties.

According to the DSC thermal analyses as displayed in Fig. 3(g)-(i), except for the GAP-TPE$_{40}$-AZO series, the GAP-TPE, GAP-TPE$_{45}$-AZO, and GAP-TPE$_{50}$-AZO series samples exhibit first-order phase transitions during the first heating scan. Endothermic events were not detected in the second cooling and heating cycles, likely due to insufficient time for

hydrogen bond recovery during these cycles. [51] The thermal absorption events detected in the first heating cycle occur near the softening point of the elastomer, which rises with the AZO ratio. A similar increasing trend was also observed for the glass transition temperature (T_g). All this data was collected in Table 1. For the unsolidified samples like GAP-TPE$_{40}$-AZO$_{10}$, GAP-TPE$_{40}$-AZO$_{20}$, and GAP-TPE$_{40}$-AZO$_{30}$, no softening temperature was detected. This is attributed to their low hard segment content, which results in fewer amide groups capable of forming intermolecular hydrogen bonds. Furthermore, after grafting AZO derivatives, hydrogen bond formation becomes even more challenging, thereby eliminating the occurrence of a detectable softening phase transition.

3.2. Two-dimensional correlation spectroscopy and curve fitting analysis

As observed in Fig. 3(d)-(f), two distinct signals appeared in the C═O characteristic region before grafting azobenzene moieties onto the GAP-TPEs. After grafting, two peaks gradually emerge in the N—H stretching region. According to previous studies [52,53], the amide structures in polyurethane (PU) form prominent inter- or intramolecular hydrogen bonds through N—H and C═O interactions. When the system is heated, the hydrogen bonds are destabilized, leading to an obvious shift in the FTIR characteristic peaks, such as the hydrogen-bonded C═O bands shift toward those of free C═O. A similar trend can also be found in the N—H stretching region.

Two-dimensional infrared (2D-IR) correlation spectroscopy facilitates the investigation of inter- and intramolecular interactions within materials by examining specific absorption bands based on FTIR spectra. [54,55] This method is widely applied in the field of polymer science, where it is used to monitor spectral perturbations caused by external factors such as temperature, composition, or pressure changes, thereby enabling the analysis of molecular interactions. [56] In the 2D-IR correlation contour map conducted in the work, red and blue zones represent positive and negative cross peaks, respectively. The 2D-IR synchronous correlation spectra are illustrated and are symmetric regarding the diagonal in the contour map. Autopeak represents the degree of correlation caused by molecular vibrational perturbations; it appears along the diagonal of the synchronous 2D-IR contour map. If any autopeak is present, a consistently positive signal at the corresponding wavenumber indicates that the spectral intensity varies under external perturbation significantly. Cross peaks are situated at the off-diagonal sites of the synchronous 2D correlation contour map; these signals can be either positive or negative, corresponding to synchronous or asynchronous changes in spectral intensity at positions ν_1 and ν_2. Under external perturbation, a positive cross peak denotes that the intensity fluctuations at ν_1 and ν_2 are positively correlated, for example, both increase or both decrease. However, negative cross peaks show the opposite directions, for instance, one increases while the other decreases. [57]

To further investigate this phenomenon, variable-temperature 2D-IR analyses were conducted on GAP-TPE$_{50}$ and GAP-TPE$_{50}$-AZO$_{30}$, representing the sample before and after the click reaction, respectively. These analyses aim to explore the thermal behavior and hydrogen bonding dynamics involving both systems as the temperature increases.

Fig. 4(a) and (b) illustrate the FTIR spectra of the C═O stretching (1630–1780 cm^{-1}) and the N—H stretching (3200–3500 cm^{-1}), respectively, for GAP-TPE$_{50}$ and GAP-TPE$_{50}$-AZO$_{30}$ under varying temperatures from 30 to 150 °C. Fig. 4(c) and (d) present the corresponding synchronous 2D-IR correlation spectra. As shown in Fig. 4(a) and (b), when the temperature increased, the peak intensity of free N—H units increased, while the peak intensity of hydrogen-bonded N—H units weakened and shifted toward higher wavenumbers. Alternatively, the peak of disordered C═O groups moved to higher wavenumbers as well, indicating a decline in the strength of hydrogen bonding. Two-dimensional correlation spectroscopy provided more effective information on hydrogen bonding interactions in these two types of

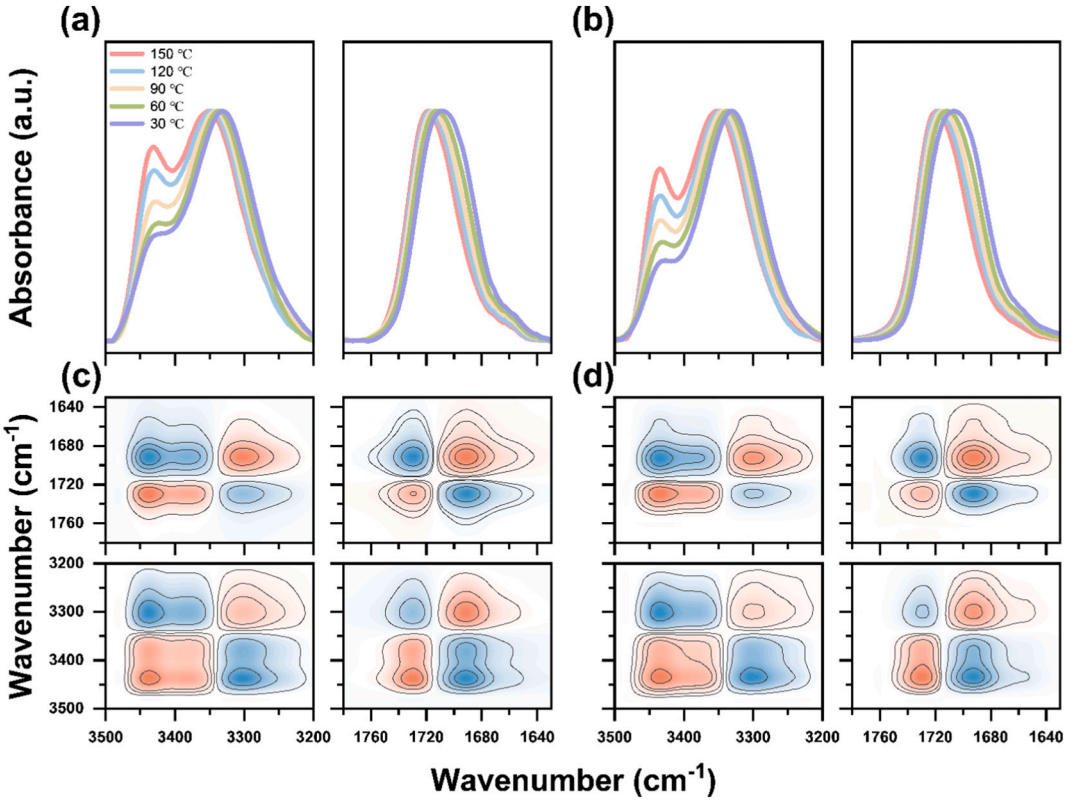

Fig. 4. Temperature-dependent IR spectra of (a) GAP-TPE$_{50}$, (b) GAP-TPE$_{50}$-AZO$_{30}$ elastomer measured at 30 °C intervals over a temperature range of 30–150 °C; Synchronous 2D contour map of (c) GAP-TPE$_{50}$ and (d) GAP-TPE$_{50}$-AZO$_{30}$ elastomers.

elastomers. In the synchronous 2D spectra (Fig. 4(c) and (d)), the wavenumbers for free N—H units appeared at 3437 cm^{-1}, while the wavenumbers for hydrogen-bonded N—H units lay in the range of 3210–3339 cm^{-1}. These two kinds of N—H units displayed a negative correlation. Similarly, the band attributed to the free C═O unit also displayed a negative correlation with those of the hydrogen-bonded C═O group, as anticipated. Additionally, the relationship between the N—H and C═O groups was also investigated. The peak of free N—H units showed a positive correlation with that of free C═O groups; likewise, the band of hydrogen-bonded N—H units exhibited a positive correlation with that of hydrogen-bonded C═O groups. Overall, the hydrogen-bonded interaction was observed in both GAP-TPE_{50} and GAP-TPE_{50}-AZO_{30} polymer.

Fig. 5 demonstrates the curve-fitting results of the C═O absorptions for GAP-TPE and GAP-TPE-AZO elastomers with different hard segment ratios. To eliminate the interference of moisture, the C═O group absorption region at 120 °C was selected for curve-fitting. The signals at 1721 and 1699 cm^{-1} correspond to free and intermolecular hydrogen-bonded C═O units, respectively. As shown in Fig. 5(a)–(c), for GAP-TPE elastomers, increasing the hard-segment content leads to a higher fraction percentage of intermolecular hydrogen-bonded C═O units, while the fraction percentage of free C═O units decreases. As observed in Fig. 5(d)–(f), GAP-TPE-AZO elastomers exhibit the same tendency, as expected. It is noteworthy that, at the same hard segment content, GAP-TPE-AZO shows a lower fraction percentage of intermolecular hydrogen-bonded C═O units compared with GAP-TPE. This is because grafting azobenzene derivatives onto the soft segment side chains increases intermolecular steric hindrance in partial regions, which interferes with hydrogen bonding between hard segments, thus reducing the fraction percentage of hydrogen-bonded C═O units.

3.3. *Photoresponsive properties and amplitude-tunable surface relief grating construction*

The formation of SRG followed the same experimental conditions as the previous study. [43] Initially, gratings and their respective diffraction efficiencies for GAP-TPE-AZO elastomers with different compositions were evaluated using a 632 nm He—Ne laser, as shown in Fig. 6(a)-(i). The number of diffraction spots was found to increase noticeably with higher AZO ratios, representing enhanced grating formation. [58] According to the number of diffraction spots, it can be strongly inferred that samples with AZO-Alkyne content above 20 wt% are capable of successfully forming surface relief gratings (SRGs). A first-order diffraction peak was observed in the sample reacting with 20 wt% AZO-Alkyne, while up to a third-order diffraction peak was detected in the 30 wt% samples. Among these, the GAP-TPE_{50}-AZO_{30} exhibited the most significant diffraction spots. Compared to the other samples, this result indicates that the formed SRG exhibits better uniformity, which enhances constructive interference. [59,60]

In addition, the change in diffraction efficiency was recorded during the SRG writing process simultaneously. No obvious measurable diffraction efficiency was observed for samples with 10 % AZO ratio, including GAP-TPE_{40}-AZO_{10}, GAP-TPE_{45}-AZO_{10}, and GAP-TPE_{50}-AZO_{10}. Then, for samples with an AZO ratio of 20 wt%, including GAP-TPE_{40}-AZO_{20}, GAP-TPE_{45}-AZO_{20}, and GAP-TPE_{50}-AZO_{20}, the diffraction efficiency remained stable during 10 to 20 min of laser exposure. The first-order diffraction efficiency peaked at 0.26 %, 0.48 %, and 0.59 %, respectively. Finally, for samples with the maximum AZO ratio of 30 wt % in this study, the highest diffraction efficiencies for each series were recorded. GAP-TPE_{40}-AZO_{30} reached its peak first-order diffraction efficiency of 4.19 % and second-order efficiency of 0.35 % after approximately 93 min of laser exposure. GAP-TPE_{45}-AZO_{30} achieved a maximum first-order efficiency of 6.37 % and a second-order efficiency of 0.93 % after around 85 min. GAP-TPE_{50}-AZO_{30} showed the highest performance, with a first-order diffraction efficiency of 7.30 % and a second-order efficiency of 1.17 % after about 115 min. These results indicated that the samples reached their maximum grating depth at these respective exposure times.

The formation of SRGs is attributed to photoinduced molecular migration driven by the spatially modulated intensity pattern of interfering with green light exposure. At constructive interference regions, molecules receive sufficient photon energy and migrate, resulting in valley formation. On the contrary, at destructive interference regions, where photon energy is weaker, molecules tend to accumulate, forming the surface grating peaks. This mass transport phenomenon is typically observed in azobenzene-containing polymers due to their photoisomerization-induced mobility under polarized light exposure. [61] Notably, GAP-TPE_{40}-AZO_{30} and GAP-TPE_{45}-AZO_{30} exhibit multiple

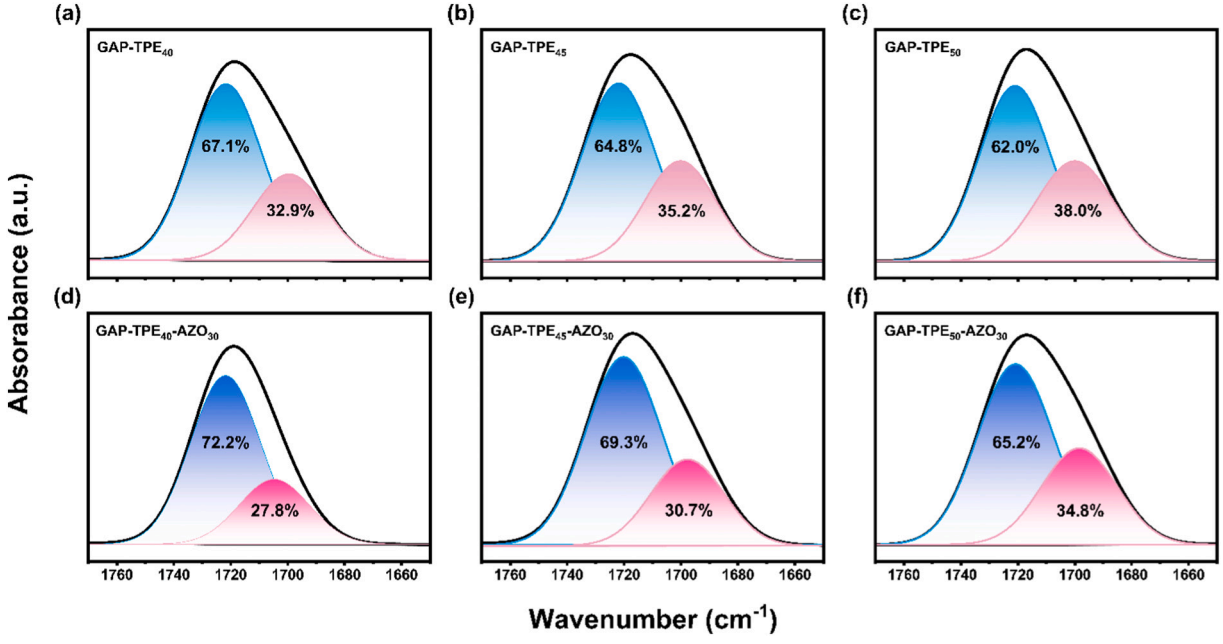

Fig. 5. Curve-fitting results of the C═O absorptions at 120 °C for (a)GAP-TPE_{40}, (b)GAP-TPE_{45}, (c)GAP-TPE_{50}, (d) GAP-TPE_{40}-AZO_{30}, (e) GAP-TPE_{45}-AZO_{30}, and (f) GAP-TPE_{50}-AZO_{30}.

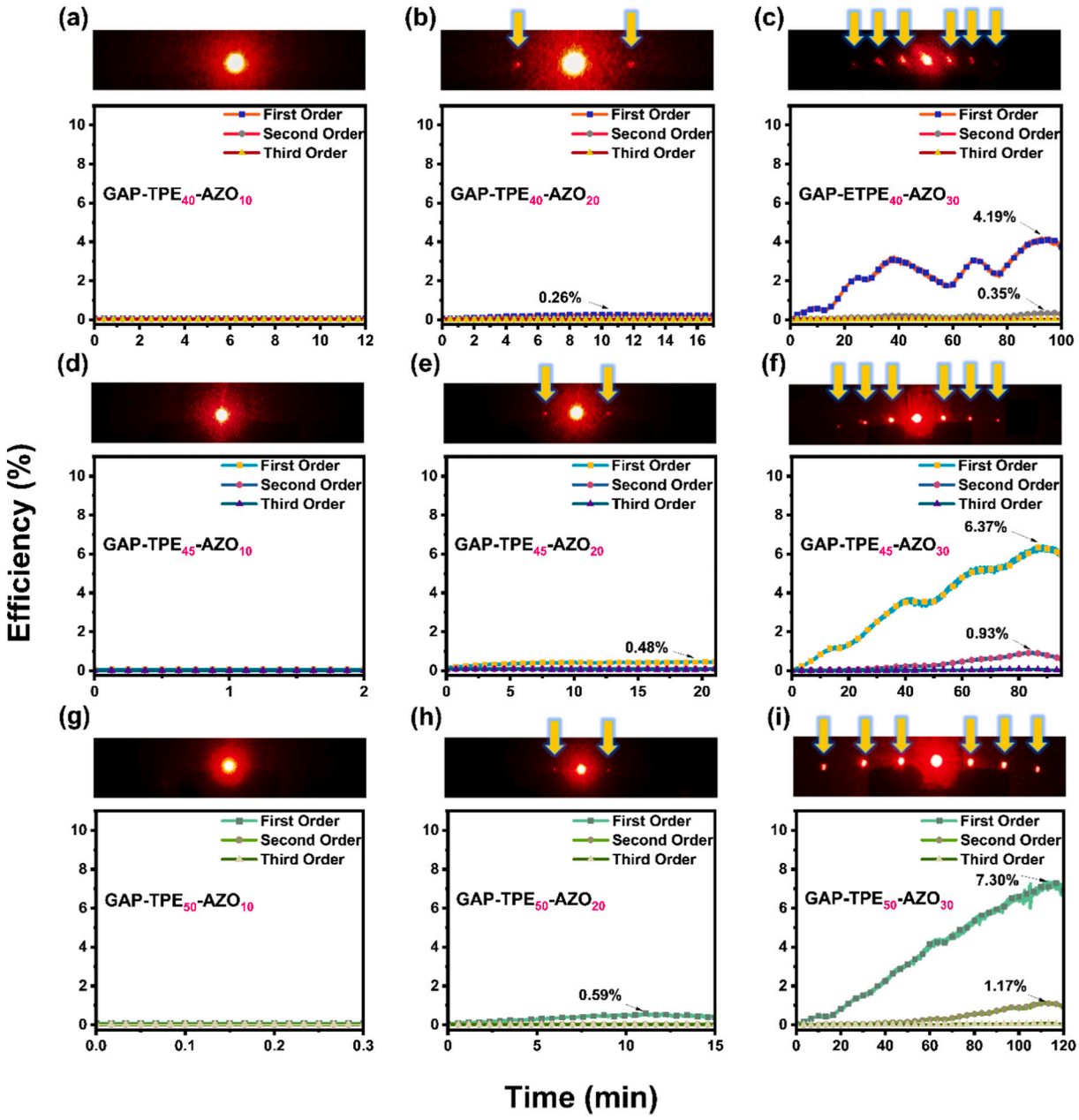

Fig. 6. Comparison of the diffraction patterns and efficiencies after the formation of grating with (a) GAP-TPE$_{40}$-AZO$_{10}$; (b) GAP-TPE$_{40}$-AZO$_{20}$; (c) GAP-TPE$_{40}$-AZO$_{30}$; (d) GAP-TPE$_{45}$-AZO$_{10}$; (e) GAP-TPE$_{45}$-AZO$_{20}$; (f) GAP-TPE$_{45}$-AZO$_{30}$; (g) GAP-TPE$_{50}$-AZO$_{10}$; (h) GAP-TPE$_{50}$-AZO$_{20}$; (i) GAP-TPE$_{50}$-AZO$_{30}$ polymers.

declines in diffraction efficiency during the writing process. This phenomenon may be attributed to the continuous absorption of photon energy by the azobenzene-grafting polymers, causing them to shift from the constructive interference areas and accumulate at the destructive interference areas. However, due to the insufficient hydrogen bonding strength between molecular chains in these stacked regions, stable solidification cannot be maintained, leading to partial molecular backflow and resulting in fluctuations in diffraction efficiency. This phenomenon is consistent with the findings in other azopolymer systems. [16]

Azobenzene undergoes photoisomerization upon absorption of suitable energy. After isomerization, the molecule can revert to its original configuration either by being kept in the dark or through thermal treatment. The isomeric structures can be distinguished based on differences in their UV/vis absorption spectra, and the degree of isomerization can be quantified by measuring changes in absorbance. However, once the azobenzene structure is constrained, such as being grafted onto a polymer or constrained within a side chain, its π orbital conjugation can be changed due to restricted conformation, leading to variations in energy levels and consequently a shift in the absorption band. [62–64] Among all the elastomer samples, GAP-TPE$_{40}$-AZO$_{30}$, GAP-TPE$_{45}$-AZO$_{30}$, and GAP-TPE$_{50}$-AZO$_{30}$ exhibited the highest diffraction efficiencies, and these elastomers were analyzed by UV/vis spectra for the isomerization degree via dissolved in THF. Under 365 nm UV irradiation, the π-π* absorption peak associated with the trans isomer at 346 nm gradually reduced with increasing exposure time. On the other hand, the n-π* absorption band corresponding to the cis isomer at 440 nm presented a slow increase, indicating a progressive trans-to-cis isomerization from azobenzene moieties. [65] As shown in Fig. S4(a)-(c), all three elastomers exhibit a significant reduction at 346 nm. Based on the change in absorbance before and after irradiation, the isomerization degree was calculated to be 87.8 % for GAP-TPE$_{40}$-AZO$_{30}$, 86.3 % for GAP-TPE$_{45}$-AZO$_{30}$, and 85.7 % for GAP-TPE$_{50}$-AZO$_{30}$. The degree of

isomerization under different irradiation durations was presented in Fig. S4(d).

The data indicated that isomerization increased with prolonged UV exposure and eventually plateaued. In addition, the maximum degree of isomerization declined slightly with increasing hard segment content in the elastomers. This trend suggests that a higher hard segment ratio results in increased molecular rigidity and reduced free volume, thus hindering the isomerization of azobenzene moieties. [62,66] One noteworthy feature of azobenzene is that the cis-to-trans isomerization is thermodynamically favored, allowing the molecule to revert to its more stable trans form over time or via heating. As shown in Fig. S4(a)-(c), while the irradiated samples were kept in the dark at room temperature, the absorption band at 346 nm gradually increased and eventually returned to its pristine intensity before irradiation, with no significant differences after approximately 140 min. As shown in Fig. S5, AFM was used to examine the surface morphology of the sample films. Before laser writing, the film exhibited a smooth surface, while after inscription, clear and regular interference fringes were observed, indicating the successful formation of SRGs. Although the elastomers containing 20 wt % AZO content exhibited first-order diffraction patterns, the diffraction efficiency was relatively low, making the resulting SRGs difficult to observe clearly. Hence, further analysis of the SRG structures formed in elastomers with 30 wt% AZO content was conducted using AFM. The surface topographies, phase diagrams, and section analysis were compared across samples with different hard segment ratios, as displayed in Fig. 7(a)–(l).

The 2D AFM images revealed regular interference fringes, and the 3D topographic images clearly presented periodic surface fluctuation with alternating peaks and valleys, confirming the successful formation of SRGs in all three samples. Using Bragg's law and considering the laser wavelength and incident angle used in this study, the theoretical grating period was calculated to be 4357 nm. As shown in Fig. 7(d), (h), and (l), the grating periods obtained from AFM cross-sectional analysis for each sample were 4367, 4323, and 4357 nm, respectively. These values deviate from the theoretical value by only −0.78 % to 0.23 %, indicating minimal error.

In tapping mode, the phase contrast is influenced by multiple factors, including the sample's energy dissipation, surface viscoelasticity, and interaction forces between tip and sample, rather than being determined by the sample's elastic modulus. Elastomers dominated by soft segments tend to bring greater energy dissipation during tip interaction, resulting in larger phase angles (brighter regions), whereas elastomers with higher hard segment content exhibit lower energy dissipation, leading to smaller phase angles (darker regions). This interpretation not only corresponds to the results demonstrated in Fig. 7(c), (g), and (k) but also aligns with the results discussed in previous research. [67,68] After SRG formation, the surface mechanical properties change locally. The grating peaks, driven by light-induced mass migration of molecules, may undergo reduced regional density and rigidity, resulting in stress redistribution. This leads to a corresponding correlation between the phase images and the surface topography of these samples.

The azobenzene content in the system is one of the critical factors influencing the grating amplitude. A higher azobenzene concentration generally results in a greater SRG amplitude. [69,70] The extreme amplitudes of the SRGs formed in GAP-TPE$_{40}$-AZO$_{30}$, GAP-TPE$_{45}$-AZO$_{30}$, and GAP-TPE$_{50}$-AZO$_{30}$ were found to be 133 nm, 488 nm, and 687 nm, respectively, as shown in Fig. 7(d), (h), and (l). However, the theoretical azobenzene ratios in the side-chain groups of these three elastomers were only slightly different at 28.0 %, 30.5 %, and 33.5 %, respectively, as listed in Table 1. Compared to the diffraction efficiencies of samples with 10 % and 20 % AZO content, the azobenzene ratio alone was insufficient to account for such a significant difference. Somewhat, the increase in hard segment ratio enhanced the proportion of hydrogen bonding association, which enabled large-scale mass migration during SRG formation. In addition, the dense hydrogen bonds further strengthened the effect in the destructive interference regions where molecular stacking occurred, leading to an increased maximum grating amplitude. This phenomenon is consistent with previous studies showing that hydrogen bonding interactions facilitate the formation of SRGs. [65,71]

Regarding durability, the evaluation of the persistence of the formed SRGs was conducted by visually observing the reflective phenomenon generated by the grating diffraction on the sample thin film (similar to the principle of anti-counterfeiting labels). Once the reflective phenomenon disappears or weakens, the grating amplitude was re-measured using AFM again to evaluate the attenuation of SRGs. The relevant data, together with the film thickness, were compiled in Table S3. The results showed that, under ambient temperature, the reflective phenomenon of the GAP-TPE$_{40}$-AZO$_{30}$ thin film sample disappeared after 3 h, and AFM measurements confirmed that the SRG had flattened and vanished. For the GAP-TPE$_{45}$-AZO$_{30}$ thin film sample, the reflective phenomenon persisted for 10 h, whereas in the GAP-TPE$_{50}$-AZO$_{30}$ thin film sample, it was still observable after more than 7 days, with AFM measurements indicating a remaining grating depth of 237 nm. These results demonstrate that the persistence of the grating increases with the hard segment content of these GAP-TPE-AZO elastomers.

SRGs formed by azobenzene-containing materials exhibit specific and reversible abilities that allow them to be repeatedly written and erased. [10,37,44] Fig. 8 demonstrates the experimental results of repeated inscription and erasure of SRGs on the GAP-TPE$_{50}$-AZO$_{30}$ elastomer. During the first inscription process, a third-order diffraction

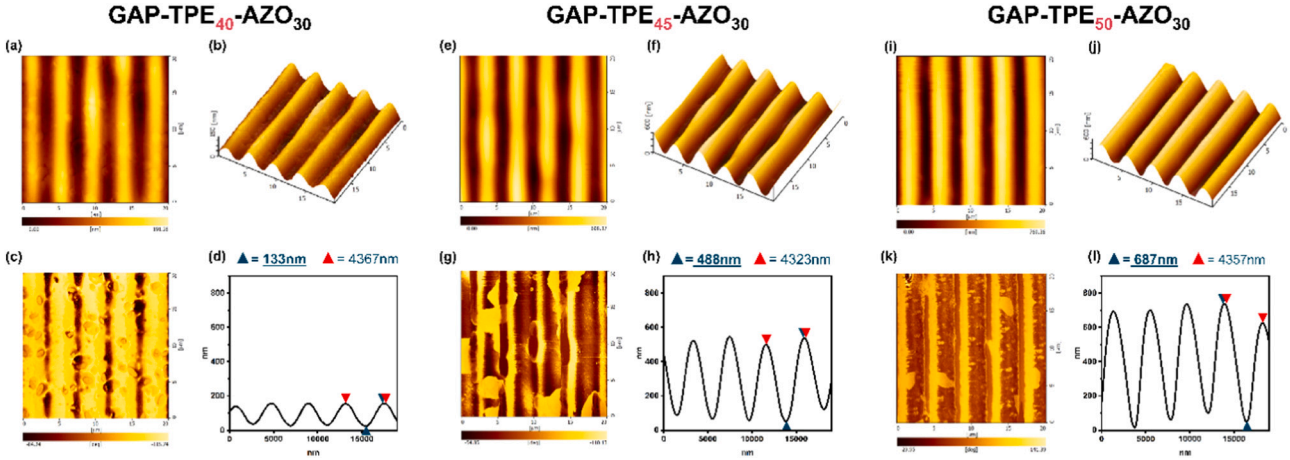

Fig. 7. 2D and 3D AFM images and section analysis of (a-d) GAP-TPE$_{40}$-AZO$_{30}$; (e-h) GAP-TPE$_{45}$-AZO$_{30}$; (i-l) GAP-TPE$_{50}$-AZO$_{30}$.

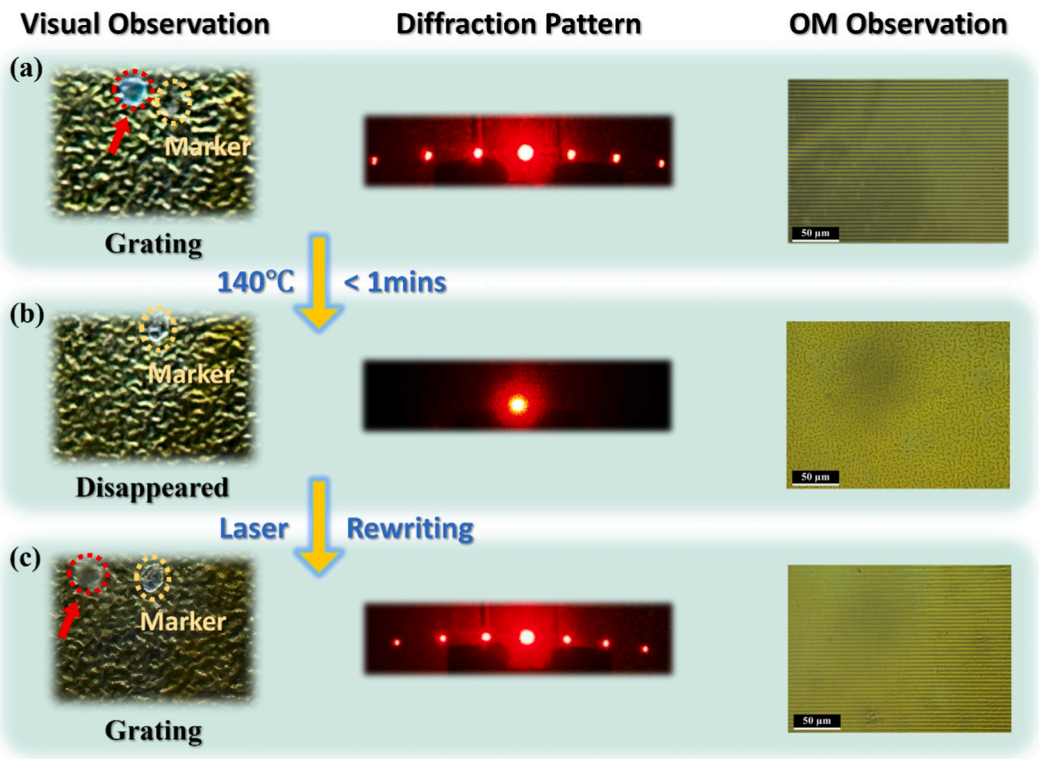

Fig. 8. Visual Observation, diffraction pattern, and OM observation results of GAP-TPE_{50}-AZO_{30} grating formation under different conditions: (a) pristine; (b) after heating at 140 °C for less than 1 min; and (c) rewriting by laser again.

pattern was clearly observed. Notably, upon heating the sample to 20 °C above its softening point to 140 °C for less than 1 min, the visible diffraction spot on the thin film disappeared. This erasure was further confirmed using optical microscopy (OM), indicating the grating structure had been successfully removed. Nevertheless, after subsequent green light exposure and rewriting, the diffraction pattern reappeared, demonstrating the rewritability of the SRG. The first-order diffraction efficiencies for the initial and second recordings were 7.3 % and 6.6 %, respectively, while the second-order efficiencies were 1.2 % and 1.3 %, as shown in Fig. S6. These values exhibited no significant difference, indicating that the SRG can be effectively rewritten without significant loss of performance. These results prove that GAP-TPE_{50}-AZO_{30} elastomers possess the capability for repeated writing and rapid erasure of SRG under simple heating conditions without additional assistance, providing strong evidence of the reversible property of the SRG formation.

4. Conclusion

In this study, thermoplastic elastomers with varying hard segment contents (GAP-TPE) were synthesized via cationic ring-opening polymerization, azide substitutions, and a straightforward polyurethane (PU) process. Azobenzene moieties were then successfully grafted onto the side chains of the elastomers in different ratios through click chemistry. The DSC profiles and UV/vis spectra confirm that the GAP-TPE-AZO_{30} series of elastomers exhibit thermoplastic properties and the ability of grafted azobenzene derivatives to undergo isomerization. A novel thermoplastic elastomer capable of forming SRG was successfully developed. The amplitude of the SRG can be finely tuned by adjusting the hard segment ratio. At hard segment ratios of 40 %, 45 %, and 50 %, the maximum grating depths measured were 133 nm, 488 nm, and 687 nm, respectively. As the hard segment content increases, the maximum grating depth also increases accordingly, indicating that a higher hard segment ratio leads to significantly larger SRG amplitudes. The ability to modulate SRG amplitude by simply varying the hard segment ratio offers a versatile and material-efficient approach to meet various application-specific demands. Furthermore, this study exploited the thermoplastic elastomer's ability to flow rapidly upon heating above its softening point, enabling fast erasure and rewritability of the SRG. This effectively overcomes the drawback of time-consuming thermal erasure under conventional heating conditions and further paves the way for expanding the application of thermoplastic elastomers in SRG-related technologies.

CRediT authorship contribution statement

Ming-Chieh Lin: Writing – original draft, Investigation, Formal analysis, Data curation, Conceptualization. **Wen-Kai Cheng:** Writing – original draft, Investigation, Formal analysis, Data curation. **Mohamed Gamal Mohamed:** Data curation, Methodology. **Wei-Hung Su:** Writing – original draft, Supervision, Resources, Methodology, Conceptualization. **Shiao-Wei Kuo:** Writing – review & editing, Writing – original draft, Supervision, Resources, Funding acquisition, Conceptualization.

Declaration of competing interest

The authors declare that they have no known competing financial interests or personal relationships that could have appeared to influence the work reported in this paper.

Acknowledgments

The study was supported by the National Science and Technology Council, Taiwan (NSTC 114-2223-E-110-001).

Appendix A. Supplementary data

Supplementary data to this article can be found online at https://doi.

org/10.1016/j.cej.2025.167803.

Data availability

No data was used for the research described in the article.

References

[1] A.H. Gelebart, D.J. Mulder, M. Varga, A. Konya, G. Vantomme, E.W. Meijer, R.L. B. Selinger, D.J. Broer, Making waves in a photoactive polymer film, Nature 546 (2017) 632–636, https://doi.org/10.1038/nature22987.

[2] K. Qian, Y. Shao, Z.R. Yang, S.M. Jiang, A multi-element encrypted and decrypted photoresponsive liquid crystal polymer network through the cooperation of cyanostilbene and spiropyran, Chem. Eng. J. 493 (2024) 152713, https://doi.org/10.1016/j.cej.2024.152713.

[3] X.T. Wang, Y.B. Yang, C. Liu, H.L. Guo, Z.F. Chen, J.Y. Xia, Y.G. Liao, C.Y. Tang, W. C. Law, Photo- and pH-responsive drug delivery nanocomposite based on o-nitrobenzyl functionalized upconversion nanoparticles, Polymer 229 (2021) 123961, https://doi.org/10.1016/j.polymer.2021.123961.

[4] Y. Shen, X.X. Le, Y. Wu, T. Chen, Stimulus-responsive polymer materials toward multi-mode and multi-level information anti-counterfeiting: recent advances and future challenges, Chem. Soc. Rev. 53 (2) (2024) 606–623, https://doi.org/10.1039/D3CS00753G.

[5] M.H. Chang, Y.C. Dzeng, Y.R. Chen, C.C. Chang, L.R. Lee, T.H. Tsai, Y.F. Chen, Y. C. Liu, T. Sugiyama, C. Chen, J.T. Chen, Polarization-driven molecular alignment of azopolymer for dual-encrypted and moiré animation-based anti-counterfeiting, Adv. Funct. Mater. (2025) 2506526, https://doi.org/10.1002/adfm.202506526.

[6] D. Gindre, A. Boeglin, A. Fort, L. Mager, K.D. Dorkenoo, Rewritable optical data storage in azobenzene copolymers, Opt. Express 14 (21) (2006) 9896–9901, https://doi.org/10.1364/OE.14.009896.

[7] P. Hu, J.H. Li, J.C. Jin, X. Lin, X.D. Tan, Highly sensitive photopolymer for holographic data storage containing methacryl polyhedral oligomeric silsesquioxane, ACS Appl. Mater. Interfaces 14 (18) (2022) 21544–21554, https://doi.org/10.1021/acsami.2c04011.

[8] S. Fredrich, T. Engels, A.P.H.J. Schenning, Multistable conventional azobenzene liquid crystal actuators using only visible light: the decisive role of small amounts of unpolymerized monomers, ACS Appl. Polym. Mater. 4 (10) (2022) 7751–7758, https://doi.org/10.1021/acsapm.2c01298.

[9] F. Reda, M. Salvatore, F. Borbone, P. Maddalena, S.L. Oscurato, Accurate morphology-related diffraction behavior of light-induced surface relief gratings on azopolymers, ACS Mater. Lett. 4 (5) (2022) 953–959, https://doi.org/10.1021/acsmaterialslett.2c00171.

[10] X. Li, H. Huang, X.G. Wang, Optical erasure and reconfiguration of surface-relief-gratings of azo polymer and azo molecular glass: a comparative study on soft-lithographic duplicates, Adv. Photon. Res. 4 (1) (2023) 2200077, https://doi.org/10.1002/adpr.202200077.

[11] C. Maria Gabriela, E. Aranxa Raquel, G. Silvia, L. Silvia Adriana, Azopolymer film as an actuator for organizing multiwall carbon nanotubes, Opt. Mater. 66 (2017) 247–252, https://doi.org/10.1016/j.optmat.2017.01.047.

[12] A.F.M. El-Mahdy, F.W. Lin, W.H. Su, T. Chen, S.W. Kuo, Photoresponsive azobenzene materials based on pyridine-functionalized benzoxazines as surface relief gratings, ACS Appl. Polym. Mater. 2 (2) (2020) 791–804, https://doi.org/10.1021/acsapm.9b01079.

[13] C.W. Huang, P.W. Wu, W.H. Su, C.Y. Zhu, S.W. Kuo, Stimuli-responsive supramolecular materials: photo-tunable properties and molecular recognition behavior, Polym. Chem. 7 (4) (2016) 795–806, https://doi.org/10.1039/C5PY01852H.

[14] C.W. Huang, W.Y. Ji, S.W. Kuo, Stimuli-responsive supramolecular conjugated polymer with phototunable surface relief grating, Polym. Chem. 9 (20) (2018) 2813–2820, https://doi.org/10.1039/C8PY00439K.

[15] O.N. Oliverira Jr., L. Li, J. Kumar, S.K. Tripathy, 14 - surface-relief gratings on azobenzene-containing films, in: S. Zouheir, K. Wolfgang (Eds.), Photoreactive Organic Thin Films, Academic Press, San Diego, 2002, pp. 429–486.

[16] F. Borbone, S.L. Oscurato, S. Del Sorbo, F. Pota, M. Salvatore, F. Reda, P. Maddalena, R. Centore, A. Ambrosio, Enhanced photoinduced mass migration in supramolecular azopolymers by H-bond driven positional constraint, J. Mater. Chem. C 9 (34) (2021) 11368–11375, https://doi.org/10.1039/D1TC02266K.

[17] M. Saphiannikova, V. Toshchevikov, N. Tverdokhleb, Optical deformations of azobenzene polymers: orientation approach vs. other concepts, Soft Matter. 20 (12) (2024) 2688–2710, https://doi.org/10.1039/D4SM00104D.

[18] J. Strobelt, S. Santer, H. Abourahma, M. Music, Z. Farzan, P. Nezamis, R. Leon, D. J. McGee, Photomechanical azopolymers and digital polarization optics: a versatile platform for surface microstructure fabrication, ACS Appl. Opt. Mater. 3 (7) (2025) 1461–1476, https://doi.org/10.1021/acsaom.5c00038.

[19] X. Li, H. Huang, B. Wu, C.Y. Liao, X.G. Wang, Comparative study of photoinduced surface-relief-gratings on azo polymer and azo molecular glass films, RSC Adv. 11 (55) (2021) 34766–34778, https://doi.org/10.1039/D1RA06111A.

[20] L.M. Goldenberg, L. Kulikovsky, O. Kulikovska, J. Stumpe, New materials with detachable azobenzene: effective, colourless and extremely stable surface relief gratings, J. Mater. Chem. 19 (43) (2009) 8068–8071, https://doi.org/10.1039/B918130J.

[21] I.M. Alarifi, A comprehensive review on advancements of elastomers for engineering applications, Adv. Indus. Eng. Polym. Res. 6 (4) (2023) 451–464, https://doi.org/10.1016/j.aiepr.2023.05.001.

[22] E.H. Backes, S.V. Harb, L.A. Pinto, N.K. de Moura, G.F. de Melo Morgado, J. Marini, F.R. Passador, L.A. Pessan, Thermoplastic polyurethanes: synthesis, fabrication techniques, blends, composites, and applications, J. Mater. Sci. 59 (4) (2024) 1123–1152, https://doi.org/10.1007/s10853-023-09077-z.

[23] U. Kalita, B. Parameswaran, N.K. Singha, Thermoplastic Elastomers, in: Kirk-Othmer Encyclopedia of Chemical Technology, John Wiley & Sons, New York, 2002, pp. 1–39.

[24] J.H. Jeon, J.H. Jung, C.R. Choi, Toward a greener future: exploring sustainable thermoplastic elastomers, J. Polym. Sci. 62 (4) (2024) 662–678, https://doi.org/10.1002/pol.20230293.

[25] S. Chen, Y.H. Wang, L. Yang, C.Z. Chu, S.C. Cao, Z. Wang, J.J. Xue, Z.W. You, Biodegradable elastomers for biomedical applications, Prog. Polym. Sci. 147 (2023) 101763, https://doi.org/10.1016/j.progpolymsci.2023.101763.

[26] S. Panja, A. Siehr, A. Sahoo, R.A. Siegel, W. Shen, Biodegradable elastomers enabling thermoprocessing below 100 °C, Biomacromolecules 23 (1) (2022) 163–173, https://doi.org/10.1021/acs.biomac.1c01197.

[27] Y.Y. Liu, M. Zhang, Y. Shen, Z.B. Li, Biodegradable and chemically recyclable thermoplastic elastomers prepared by ring-opening polymerization of cyclic monomers, Polym. Sci. Technol. (2025), https://doi.org/10.1021/polymscitech.5c00050.

[28] A. Schade, M. Melzer, S. Zimmermann, T. Schwarz, K. Stoewe, H. Kuhn, Plastic waste recycling—a chemical recycling perspective, ACS Sustain. Chem. Eng. 12 (33) (2024) 12270–12288, https://doi.org/10.1021/acssuschemeng.4c02551.

[29] P.K. Behera, S. Dhamaniya, S. Mohanty, V. Gupta, Chapter 16 - advances in thermoplastic polyurethane elastomers: Design, applications and their circularity, in: N.K. Singha, S.C. Jana (Eds.), Advances in Thermoplastic Elastomers, Elsevier, Amsterdam, 2024, pp. 407–444, https://doi.org/10.1016/B978-0-323-91758-2.00014-3.

[30] X.X. Zhang, L.P. Wang, K.Q. Zhang, K.Y. Zhou, K.Y. Hou, Z.X. Zhao, G.L. Li, Q. Yao, N. Sun, X. Wang, Hybrid soft segments boost the development of ultratough thermoplastic elastomers with tunable hardness, Adv. Mater. 37 (15) (2025) 2414720, https://doi.org/10.1002/adma.202414720.

[31] H.Z. Luo, H.H. Deng, Y.Y. Zhu, H.B. Shi, C.Q. Zhang, Y. Wang, High-performance polyurethane elastomers with mechano-responsive self-reinforcing via rigid-flexible segments regulation, Compos. Part B Eng. 297 (2025) 112287, https://doi.org/10.1016/j.compositesb.2025.112287.

[32] M. Asensio, J.F. Ferrer, A. Nohales, M. Culebras, C.M. Gómez, The role of diisocyanate structure to modify properties of segmented polyurethanes, Materials 16 (4) (2023) 1633, https://doi.org/10.3390/ma16041633.

[33] M. Fuensanta, J.M. Martín-Martínez, Structural and viscoelastic properties of thermoplastic polyurethanes containing mixed soft segments with potential application as pressure sensitive adhesives, Polymers 13 (18) (2021) 3097, https://doi.org/10.3390/polym13183097.

[34] C.H. Wu, C.W. Chen, P.H. Chen, Y.S. Chen, F.S. Chuan, S.P. Rwei, Characteristics of polycarbonate soft segment-based thermoplastic polyurethane, Appl. Sci. 11 (12) (2021) 5359, https://doi.org/10.3390/app11125359.

[35] N. Sabahi, I. Roohani, C.H. Wang, E. Farajzadeh, X.P. Li, Thermoplastic polyurethane-based shape memory polymers with potential biomedical application: the effect of TPU soft-segment on shape memory effect and cytocompatibility, Polymer 283 (2023) 126189, https://doi.org/10.1016/j.polymer.2023.126189.

[36] B.X. Liu, Z.H. Niu, Z.L. Wang, Y.M. Wang, H. Zou, X.Y. Zhao, S.K. Hu, Effect of hard segment content on the phase separation and properties of hydroxyl-terminated polybutadiene thermoplastic polyurethane, Polym. Test. 143 (2025) 108681, https://doi.org/10.1016/j.polymertesting.2024.108681.

[37] S.W. Kuo, H.T. Tsai, Control of peptide secondary structure on star shape polypeptides tethered to polyhedral oligomeric silsesquioxane nanoparticle through click chemistry, Polymer 51 (24) (2010) 5695–5704, https://doi.org/10.1016/j.polymer.2010.10.005.

[38] A. Tofini, L. Levesque, O. Lebel, R.G. Sabat, Erasure of surface relief gratings in azobenzene molecular glasses by localized heating using a CO_2 laser, J. Mater. Chem. C 6 (5) (2018) 1083–1091, https://doi.org/10.1039/C7TC05590K.

[39] T.S. Lee, D.Y. Kim, X.L. Jiang, L. Li, J. Kumar, S. Tripathy, Photoinduced surface relief gratings in high-Tg main-chain azoaromatic polymer films, J. Polym. Sci. A Polym. Chem. 36 (2) (1998) 283–289, https://doi.org/10.1002/(SICI)1099-0518(19980130)36:2<283::AID-POLA11>3.0.CO;2-K.

[40] X. Li, H. Huang, B. Wu, C.Y. Liao, X.G. Wang, Comparative study of photoinduced surface-relief-gratings on azo polymer and azo molecular glass films, RSC Adv. 11 (55) (2021) 34766–34778, https://doi.org/10.1039/D1RA06111A.

[41] C.W. Huang, F.C. Chang, Y.L. Chu, C.C. Lai, T.E. Lin, C.Y. Zhu, S.W. Kuo, A solvent-resistant azide-based hole injection/transporting conjugated polymer for fluorescent and phosphorescent light-emitting diodes, J. Mater. Chem. C 3 (31) (2015) 8142–8151, https://doi.org/10.1039/C5TC01794G.

[42] A. Stribeck, E. Pöselt, B. Eling, F. Jokari-Sheshdeh, A. Hoell, Thermoplastic polyurethanes with varying hard-segment components. Mechanical performance and a filler-crosslink conversion of hard domains as monitored by SAXS, Eur. Polym. J. 94 (2017) 340–353, https://doi.org/10.1016/j.eurpolymj.2017.07.020.

[43] Z.H. Wang, C.D. Wang, X.L. Zhao, X.N. Yang, Manipulating the mechanical properties of thermoplastic polyurethane via regulating hard segment aggregation, Macromolecules 58 (9) (2025) 4394–4406, https://doi.org/10.1021/acs.macromol.5c00142.

[44] C.W. Huang, L.Z. Huang, M.T. Hung, M.G. Mohamed, A.F.M. El-Mahdy, S.W. Kuo, Creating supramolecular functional materials via nucleobase interaction: investigating molecular recognition and the fabrication of surface relief gratings, ACS Appl. Polym. Mater. 6 (1) (2024) 732–745, https://doi.org/10.1021/acsapm.3c02354.

[45] M.Y. Tsai, M.C. Lin, S.Y. Hong, Y.C. Wu, M.G. Mohamed, S.W. Kuo, Rational design of glycidyl azide polymer-based triblock copolymers for high-performance energetic thermoplastic elastomers, Polymer 327 (2025) 128403, https://doi.org/10.1016/j.polymer.2025.128403.
[46] A.M. Kawamoto, J.A.S. Holanda, U. Barbieri, G. Polacco, T. Keicher, H. Krause, M. Kaiser, Synthesis and characterization of glycidyl azide-r-(3,3-bis(azidomethyl) oxetane) copolymers, Propellants Explos. Pyrotech. 33 (5) (2008) 365–372, https://doi.org/10.1002/prep.200700221.
[47] B.Y. Ryu, T. Emrick, Thermally induced structural transformation of bisphenol-1,2,3-triazole polymers: smart, self-extinguishing materials, Angew. Chem. Int. Ed. 49 (50) (2010) 9644–9647, https://doi.org/10.1002/anie.201005456.
[48] K. Ramya, R. Shanmugam, S. Latha, R. Sahana, P. Mounica, A. Elangovan, G. Arivazhagan, Self-associates of 1,2,4-triazole: FTIR studies, quantum chemical calculations and topological analysis, J. Mol. Struct. 1316 (2024) 138926, https://doi.org/10.1016/j.molstruc.2024.138926.
[49] S.W. Kuo, Hydrogen Bonding in Polymeric Materials, first ed, John Wiley & Sons, New Jersey, 2018.
[50] M. Asensio, V. Costa, A. Nohales, O. Bianchi, C.M. Gómez, Tunable structure and properties of segmented thermoplastic polyurethanes as a function of flexible segment, Polymers 11 (12) (2019) 1910, https://doi.org/10.3390/polym11121910.
[51] R.H. Lambeth III, M.H. Baranoski, A.M. Savage, B.F. Morgan, F.L. Beyer, B. A. Mantooth, N.E. Zander, Synthesis and characterization of segmented polyurethanes containing trisaminocyclopropenium carbocations, ACS Macro Lett. 7 (7) (2018) 846–851, https://doi.org/10.1021/acsmacrolett.8b00395.
[52] H.R. Wang, L. Cao, X.L. Wang, X.R. Lang, W.W. Cong, L. Han, H.Y. Zhang, H. B. Zhou, J.J. Sun, C.Z. Zong, Effects of isocyanate structure on the properties of polyurethane: synthesis, performance, and self-healing characteristics, Polymers 16 (21) (2024) 3045, https://doi.org/10.3390/polym16213045.
[53] E. Wittenberg, A. Meyer, S. Eggers, V. Abetz, Hydrogen bonding and thermoplastic elastomers – a nice couple with temperature-adjustable mechanical properties, Soft Matter 14 (14) (2018) 2701–2711, https://doi.org/10.1039/C8SM00296G.
[54] S.W. Kuo, Hydrogen bonding interactions in polymer/polyhedral oligomeric silsesquioxane nanomaterials, J. Polym. Res. 29 (2) (2022) 69, https://doi.org/10.1007/s10965-021-02885-4.
[55] Y.C. Kao, Y.H. Ku, M.G. Mohamed, W.H. Su, S.W. Kuo, Microphase separation transformation in bio-based benzoxazine/phenolic/PEO-b-PCL diblock copolymer mixtures induced by transesterification reaction, Macromolecules 58 (1) (2025) 585–600, https://doi.org/10.1021/acs.macromol.4c02072.
[56] Y. Park, I. Noda, Y.M. Jung, Two-dimensional correlation spectroscopy in polymer study, Front. Chem. 3 (2015), https://doi.org/10.3389/fchem.2015.00014.
[57] I. Noda, Y. Ozaki, Principle of two-dimensional correlation spectroscopy, in: I. Noda, Y. Ozaki (Eds.), Two-Dimensional Correlation Spectroscopy – Applications in Vibrational and Optical Spectroscopy, John Wiley & Sons, New Jersey, 2004, pp. 15–38.
[58] B.W. Yang, Y.F. Ji, F. Cai, H.F. Yu, Surface morphing of azopolymers toward advanced anticounterfeiting enabled by a two-step method: light writing and then reading in liquid, ACS Appl. Mater. Interfaces 15 (19) (2023) 23804–23812, https://doi.org/10.1021/acsami.3c03807.
[59] D.W. Ni, D.W. Cheng, Y. Liu, X.M. Wang, C. Yao, T. Yang, C. Chi, Y.T. Wang, Uniformity improvement of two-dimensional surface relief grating waveguide display using particle swarm optimization, Opt. Express 30 (14) (2022) 24523–24543, https://doi.org/10.1364/OE.462384.
[60] A. Zia, H.R. Wu, S. Saeed, T.L. Man, H.M. Liu, C.X. Chen, Y.H. Wan, Three-layer polarisation volume grating with enhanced diffraction efficiency and FOV in AR and VR applications, Liq. Cryst. (2024) 1–10, https://doi.org/10.1080/02678292.2024.2419943.
[61] D.Y. Kim, S.K. Tripathy, L. Li, J. Kumar, Laser-induced holographic surface relief gratings on nonlinear optical polymer films, Appl. Phys. Lett. 66 (10) (1995) 1166–1168, https://doi.org/10.1063/1.113845.
[62] C. Shang, Z.Q. Xiong, S.J. Liu, W. Yu, Molecular dynamics of azobenzene polymer with photoreversible glass transition, Macromolecules 55 (9) (2022) 3711–3722, https://doi.org/10.1021/acs.macromol.2c00073.
[63] R.C. Lan, J. Sun, C. Shen, R. Huang, Z.P. Zhang, C. Ma, J.Y. Bao, L.Y. Zhang, L. Wang, D.K. Yang, H. Yang, Light-driven liquid crystalline networks and soft actuators with degree-of-freedom-controlled molecular motors, Adv. Funct. Mater. 30 (19) (2020) 2000252, https://doi.org/10.1002/adfm.202000252.
[64] S.D. Sun, S.F. Liang, W.C. Xu, G.F. Xu, S. Wu, Photoresponsive polymers with multi-azobenzene groups, Polym. Chem. 10 (32) (2019) 4389–4401, https://doi.org/10.1039/C9PY00793H.
[65] M.T. Hung, C.W. Huang, Hydrogen bonding-mediated supramolecular blend for the fabrication of amplitude-controllable surface relief gratings, ACS Appl. Polym. Mater. 6 (14) (2024) 8200–8209, https://doi.org/10.1021/acsapm.4c01123.
[66] C. Wallace, K. Griffiths, B.L. Dale, S. Roberts, J. Parsons, J.M. Griffin, V. Görtz, Understanding solid-state photochemical energy storage in polymers with azobenzene side groups, ACS Appl. Mater. Interfaces 15 (26) (2023) 31787–31794, https://doi.org/10.1021/acsami.3c04631.
[67] R. Garcia, Nanomechanical mapping of soft materials with the atomic force microscope: methods, theory and applications, Chem. Soc. Rev. 49 (16) (2020) 5850–5884, https://doi.org/10.1039/D0CS00318B.
[68] B. Rajabifar, G.F. Meyers, R. Wagner, A. Raman, Machine learning approach to characterize the adhesive and mechanical properties of soft polymers using peakforce tapping AFM, Macromolecules 55 (19) (2022) 8731–8740, https://doi.org/10.1021/acs.macromol.2c00147.
[69] T. Fukuda, H. Matsuda, T. Shiraga, T. Kimura, M. Kato, N.K. Viswanathan, J. Kumar, S.K. Tripathy, Photofabrication of surface relief grating on films of azobenzene polymer with different dye functionalization, Macromolecules 33 (11) (2000) 4220–4225, https://doi.org/10.1021/ma991803d.
[70] V. Börger, O. Kuliskovska, K.G. Hubmann, J. Stumpe, M. Huber, H. Menzel, Novel polymers to study the influence of the azobenzene content on the photo-induced surface relief grating formation, Macromol. Chem. Phys. 206 (15) (2005) 1488–1496, https://doi.org/10.1002/macp.200500147.
[71] A. Priimagi, K. Lindfors, M. Kaivola, P. Rochon, Efficient surface-relief gratings in hydrogen-bonded polymer-azobenzene complexes, ACS Appl. Mater. Interfaces 1 (6) (2009) 1183–1189, https://doi.org/10.1021/am9002149.